CHAPTER 4

Accepted manuscript.
Comment: The printed version was modified from British to US English.

Cite as:
Alexakis, H., Cocking, S., Tziavos, N. I., Din-Houn Lau, F., Schooling, J. & DeJong, M. (2023) 'Sensor-based structural assessment of aging bridges', In Noori, M., Rainieri, C., Domaneschi, M. & Sarhosis, V. (eds.) *Data Driven Methods for Civil Structural Health Monitoring and Resilience: Latest Developments and Applications*. CRC Press, pp. 76-97

Sensor-based structural assessment of ageing bridges

Haris Alexakis* https://orcid.org/0000-0002-6588-2070

Sam Cocking https://orcid.org/0000-0003-2782-3464

Nikolaos I. Tziavos https://orcid.org/0000-0002-3692-9626

F. Din-Houn Lau https://orcid.org/0000-0003-1065-828X

Jennifer Schooling https://orcid.org/0000-0002-4777-0438 and

Matthew DeJong https://orcid.org/0000-0002-6195-839X

* corresponding author, c.alexakis@aston.ac.uk

Abstract:

Transport infrastructure managers need to ensure longevity of their networks to meet pressing sustainability demands. Extending the operational life of complex structural systems, such as ageing bridges, requires a comprehensive life-expectancy assessment. Given that these structures are suffering from local failures that may not necessarily alter their global response, engineers need to increase their confidence in detecting and characterising such damage, while assessing deterioration rates in localised regions.

This chapter presents data analysis results from the structural health monitoring of three ageing bridges: two masonry arch rail bridges, and a half-joint concrete motorway bridge. The aim, in all cases, is to improve deterioration assessment through enhanced sensing of the distributed response across the structures. A core sensing technology used in the three schemes is the development of fibre Bragg grating (FBG) networks, allowing the study of small dynamic strain variations at both the local and global response level. New ways of installing FBGs are explored for multi-aspect condition monitoring, while their sensitivity in damage detection is enhanced with data analytics and acoustic emission sensors. The chapter discusses that complementing information from dynamic strain and acoustic emission sensing networks may enable a finer deterioration monitoring of ageing structures driven by data.

CHAPTER 4

4.1. Introduction

Infrastructure managers need to improve the performance and longevity of existing structures to reduce carbon emissions and meet increased sustainability demands. Bridges are vital transport assets where a serviceability concern could lead to prolonged travel and economic disruptions. While ensuring their resilience is essential for the public's safety and prosperity, there are significant uncertainties regarding their structural performance, especially for old bridges that were designed using poorly detailed standards and practices.

In particular, national design standards for bridges were first introduced as late as the 1960s (BSI, 1962), while wider cross-national standardisation efforts started in 1975 by the European Commission led to the publication of the first Eurocodes in 1984. The transition period of the 60s-80s marked an era of wide standardisation of building codes, which improved the structural quality and performance of bridges while overlooking life-cycle management and sustainability aspects. This has raised concerns for the future of existing bridges, which deteriorate exponentially as they approach their design life expectancy, typically limited to 100-120 years.

Bridges constructed during the 60s-80s transition period, occasionally with poor practices, have already reached the second half of their expected operational life as defined in modern codes. Furthermore, a significant number of bridges still in use were constructed much earlier, without design life specifications, especially in railways. For instance, the number of masonry arch bridges and culverts in Europe was estimated to exceed 200,000, corresponding to more than 50% of the total railway bridge stock (Orbán, 2004). Most of these structures have been in operation for more than a century and experience significantly increased operational loads today.

Ageing bridges designed with poor standards are of particular concern, as their true operational life expectancy is typically unknown. The vast number of ageing structures in transport networks, their unknown structural details, the complexity of structural systems and deterioration mechanisms, and the relative recent adoption of sustainability goals (UN, 2017) are just some of the reasons explaining the lack of standardisation in infrastructure maintenance guidelines, as opposed to design standards. Currently, there are only a few examples of such international standards, which have been developed mostly by individual transport managers (UIC 778-4, 2009).

Moreover, there is an urgent need to deepen our knowledge of the performance of deteriorating structures and reduce the uncertainties regarding their behaviour. This uncertainty and absence of standardisation has led to data protectiveness and lack of transparency (in most cases) between stakeholders, as well as poor availability of tools and regulations to support the development of collaborative frameworks that could prevent catastrophic structural failures, such as the Morandi bridge collapse (Calvi et al., 2019). Additionally, this has led to further barriers to the inclusion of new technologies in standards, which further impedes investment in novel digital maintenance technologies and delays infrastructure digitalisation.

In this uncertain environment, infrastructure managers are searching for comprehensive structural assessment tools to optimise maintenance and operational decisions in their transport networks. Various techniques have been proposed to assess the structural condition of civil infrastructure. Noteworthy developments in the field of Structural Health Monitoring (SHM) include modal-based damage detection, which offers a promising alternative for remote asset management of flexible structures such as long-span bridges (Kaloop and Hu, 2015; Santos et al., 2016). Separately, a wide range of digital technologies for surveying ('from distance') and monitoring can now detect geometric anomalies and cracks, offering tools for rapid assessment (Acikgoz et al., 2017; Acikgoz et al., 2018a; Chaiyasarn et al., 2018). Nevertheless, most steel, concrete and masonry infrastructure are stiff structures suffering from local deterioration that initially does not affect global performance or response. Masonry bridges suffer from localised failures (e.g., arch ring separation/delamination, and spandrel-arch barrel separation) that may induce, at a later stage, partial or global collapse mechanisms. Furthermore, internal reinforcement corrosion is the dominant deterioration mode of concrete bridges. For instance, 66% of deteriorating bridges in Japan are found to suffer mostly from chloride ingress, and 5% from carbonation/alkalinity decrease (Mutsuyoshi, 2001). What is common in all these damage modes is that (a) early detection is crucial to ensure bridge serviceability, public safety, and reduced repair cost, and (b) such local/underlying damage does not necessarily manifest itself in the global measures of performance or at the material surface (De Santis and Tomor, 2013; Behnia et al. 2014; Alexakis et al. 2021) until the deterioration is extensive and often beyond repair. Hence, a much finer level of deterioration monitoring is necessary to assess the detailed performance state and deterioration rate of ageing bridges and to intervene in a timely fashion.

This work presents data analysis results from three ageing bridge SHM projects: two masonry arch rail bridges and one concrete motorway bridge. In all three cases, the central idea is the development of high-sensitivity sensing networks able to provide information on multiple aspects of the structural response, distributed across large critical elements, such as masonry arch barrels or concrete half-joint supports. A core technology used in all bridges for the creation of these networks is fibre Bragg grating (FBG) sensing, in which the fibres are externally attached via a system of aluminium clamps. New ways of installing FBGs are explored in the three projects to capture different structural response aspects under train or traffic loading, such as local crack behaviour, 3-dimensional arch barrel deformation and identification of collapse mechanisms, out-of-plane arch ‘pumping’, and dynamic deformation of half-joint supports. Identification of mechanical damage is enhanced by introducing new statistical modeling and machine learning for Civil SHM to detrend the effect of small train loading and ambient temperature variations. Information regarding local material degradation is enhanced with Acoustic Emission (AE) sensing, which is shown to be a complementary sensing technique to strain-based monitoring, as it may provide critical information on the deterioration rate and the likelihood of imminent brittle failures. This chapter discusses that complementary sensing networks could enable data-driven damage assessment of complex ageing infrastructure systems, reducing the uncertainties for infrastructure managers regarding the state and deterioration rate of their assets.

4.2. The Marsh Lane Viaduct

4.2.1. Sensing network and installation novelties

The Marsh Lane Viaduct is located at the Eastern entrance of the central railway station in Leeds, UK, carrying two electrified rail tracks. It was constructed between 1865 and 1869. Fig. 1 shows the northern view of the investigated section of the viaduct, comprising Arches #37, #38 and #39 (from right to left), while Fig. 2 is the plan view highlighting the main visible cracks of the arch barrels.

Figure 1. Northern view of the Marsh Lane Viaduct in Leeds, UK.

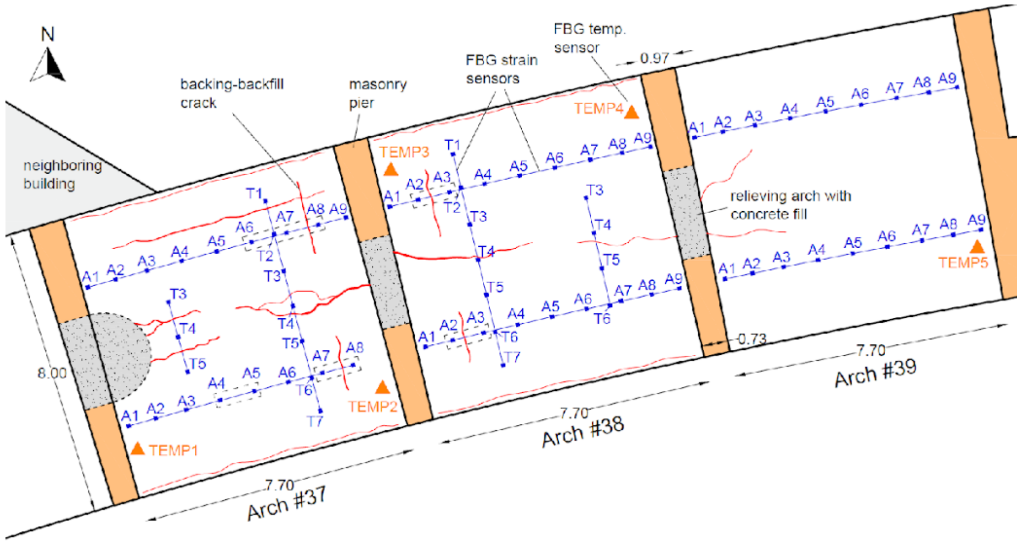

Figure 2. Plan view of Arches #37-39, showing the main damages and FBG sensor locations

Figure 3. FBG strain sensors in Arch #37

The main damages are concentrated above the relieving arches of the piers, especially between Arches 37 and 38, due to a sagging mechanism that forces the relieving-arch keystone to descend and the pier walls to bow outwards (Acikgoz et al. 2018b). This has caused bending cracks that developed along the longitudinal direction from the relieving arches up to the arch-vault keystones (Fig. 2). Another longitudinal crack has developed in Arch #37 below the North rail track. In addition, cracks in the transverse direction are observed at four symmetric locations around the pier between Arches #37 and #38 at the height where the rigid internal backing meets the backfill (Alexakis et al. 2019a). In an effort to arrest further degradation in these locations, Arches #37-39 were repaired in 2015 by the bridge owner, Network Rail, who filled in the relieving arches with concrete and installed steel ties in the transverse direction to confine the piers and spandrel walls.

Fig. 2 indicates, with blue colour, the installation of the FBG network. The small squares represent the aluminum clamps used to externally attach the fibre optic cables, also shown in Fig. 3 for Arch #37. The FBG strain sensors are located between the clamps at a spacing of 1m, monitoring dynamic strain at a 1 kHz sampling rate (further sensors and system specs are provided in Alexakis et al. 2019b). The FBG arrays were installed in both the longitudinal and transverse directions to intersect perpendicularly with the main transverse and longitudinal cracks, respectively, and thus monitor their behaviour. Steel cords with attached FBG sensors were installed between the arch springings, below the longitudinal FBG arrays, to monitor the pier-to-pier arch span opening response.

Having two FBG arrays in each direction has allowed the study of the 3D dynamic deformation of the vaults during train loading, uncovering the main response mechanisms reported in Acikgoz et al. (2018b). Furthermore, installing FBG arrays in the longitudinal direction, below the two rail tracks, has been particularly useful for train loading identification and classification (Alexakis et al. 2021). For instance, Fig. 4 presents typical responses of sensor "37NA5A6", which is located in the North FBG array of Arch #37, between clamps A5 and A6 (see Figs. 2, 3), under the most common passenger trains. In Fig. 4, the number of positive peaks corresponds to the number of axles, which permits train classification based on the number of cars by means of peak detection analysis. Furthermore, having sensors at symmetric longitudinal locations in subsequent arch spans allows for cross-correlation of signals from different arches to identify time lags, and hence the train speed and direction (Alexakis et al. 2021).

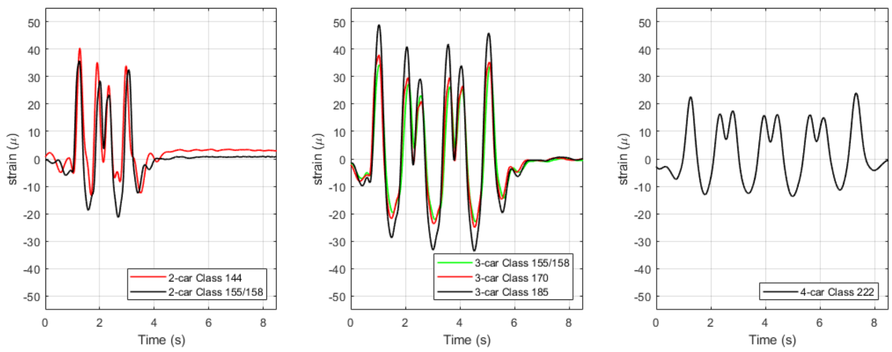

Figure 4. Response of the FBG sensor "37NA5A6", located in the North FBG array of Arch #37, between clamps A5 and A6, for the most common passenger trains with two cars (left), three cars (center) and four cars (right)

This preliminary train classification allowed the study of statistical variations in the dynamic deformation of the bridge along the FBG network based on the same train loading, and in particular the 3-car passenger trains that represent around 50% of all data. The analysis indicated 5 locations where the strain response has been amplified over a period of two years, between 2016 and 2018. These locations are the four transverse cracks and south keystone area of the most damaged arch, Arch #37, indicated in dashed-line boxes in Fig. 2. In all other locations, relatively uniform strain variations were observed, following seasonal temperature fluctuation (Alexakis et al. 2019c).

This analysis so far has not considered small train loading variations within the same type of passenger train. For instance, Fig. 4-centre shows three different 3-car passenger train classes that result in similar responses, which were hard to distinguish in practice. To do so requires a finer signal classification analysis, which would be able to detrend small response changes, caused by train loading and environmental effect variations, and would lead to enhanced mechanical damage detection.

4.2.2. Statistical shape analysis and results

Our analysis proceeds with a dataset that consists of $M = 1151$ 3-carriage train passage events heading East that occurred between July 2016 and March 2019. All events have dynamic strain and temperature data from the FBG network, apart from the first 31 events in July 2016 (preliminary dataset) where FBG temperature sensors where not available; for those events the temperature was taken from the Leeds Weather Archive of the National Centre for Atmospheric Science database (Alexakis et. al 2021).

In order to analyse the bridges' behaviour at a sensor location, a method is required to compare train passage events. In our original paper (Alexakis et. al 2021), a modified procedure of Ordinary Procrustes Analysis (OPA), a key transformation in Statistical Shape Analysis (Dryden and Mardia, 2016), is used to transform one *shape* of dynamic strain values onto another. A shape is described by a finite number of points called landmarks – see Fig. 5 for an example train passage event with landmarks. The modified OPA approach transforms one set of landmarks onto another. More precisely, the transformation from landmarks X (a matrix) onto Y (another matrix) is given by minimizing

$$D^2(X,Y) = ||Y - \beta \circ X - 1_{15}\gamma||^2 \qquad (4.1)$$

over $\beta = (\beta_1, \beta_2)$ and γ, where $||X|| = \sqrt{trace(X^T X)}$ and $\circ$ is the Hadamard product. Minimising Eq. 4.1 is straightforward and more importantly leads to interpretable results.

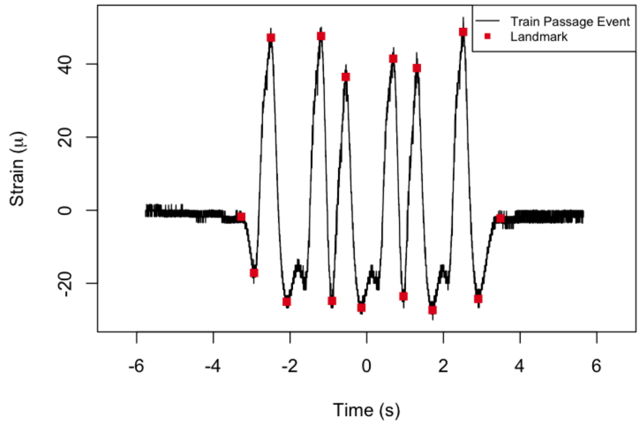

Figure 5. Dynamic strain readings from a train passage event from sensor location 37NA6A7 along with landmarks.

To assess changes in the bridges' response at a particular sensor location, all $M = 1151$ events are transformed onto the first chronological event using Eq. 4.1. This transformation gives the set of estimates $\{\hat{\beta}_1(j), \hat{\beta}_2(j), \hat{\gamma}(j); j = 1, \ldots, M\}$. The estimates have the following interpretation: $\hat{\beta}_1(j)$ is the amount of time-scaling required to map the first chronological event onto the jth train passage event. Similarly, $\hat{\beta}_2(j)$ is the amount of strain-scaling required to map the first chronological event onto the jth event. (The parameter γ and its estimate is not of interest in this application.) Thus, the estimated values allow us to compare the shape in FBG signals relative to the first train passage event record at a given sensor location. Comparing dynamic strain values from train events using this modified OPA approach is novel. Typically, events are summarised by a single extreme value such as the maximum strain value, as in previous studies (Alexakis et al. 2019a-c). The modified OPA approach uses the strain values from the landmark locations giving a broader view of the shape of the dynamic strain response. Moreover, the parameters from the modified OPA approach have meaningful interpretations of direct import to structural health monitoring. In particular, $\hat{\beta}_1$ represents variation in train speed, and $\hat{\beta}_2$ variation in strain amplitude.

A plot of the estimate strain-scaling values, $\hat{\beta}_2(j)$, against temperature (see Fig. 6-left), reveals two patterns: as temperature increases, the $\hat{\beta}_2$ value generally decreases; and the magnitude of the $\hat{\beta}_2$ value depends on some latent groups in the data which are suggested by partitioning lines in Fig. 6-left. Note that the preliminary 31 events in 2016 have estimated temperature records, and that $\hat{\beta}_1(j)$, relating to train speeds, did not show any pattern over time, with temperature or with $\hat{\beta}_2$.

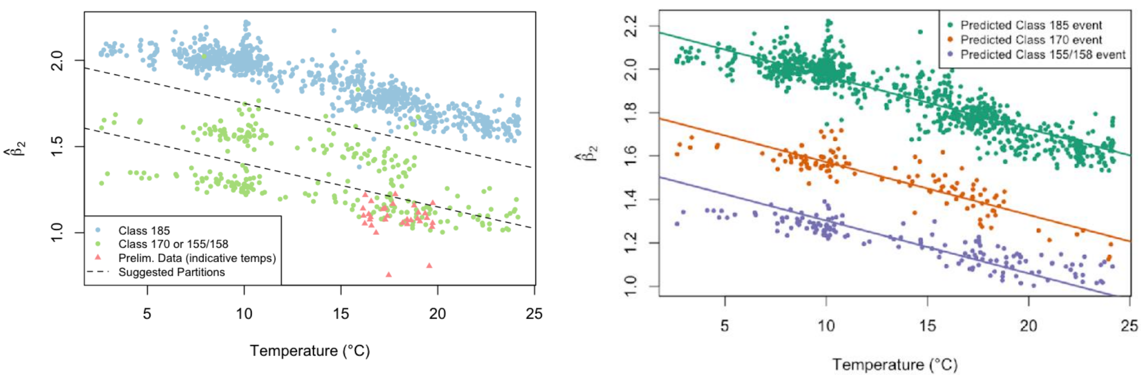

Figure 6. Left – Strain-scaling values, $\hat{\beta}_2(j)$; j=1,…,M against temperature. Suggested groups of data are indicated by the separating partition dashed lines. Right – Predicted train class labels given by SVM (coloured dots), along with expected strain-value values (coloured lines) given by a linear model.

The patterns, presented in Fig 6-left, are captured and predicted using a statistical model, which can be used for damage detection. In order to develop a representative model, the latent groups first need to be labelled. This is achieved using a supervised classification method called a support vector machine (SVM) (Cortes and Vapnik 1995). The latent groups correspond to a large extent with the different train classes.

First, a SVM is used to classify the two classes of train, (i) Class 185 (heavier, more frequent train) and (ii) Class 155/158 or 170 (lighter, less frequent trains), using the $\hat{\beta}_2(j)$ and temperature value of each train passage event. The preliminary dataset was excluded since no temperature records exist. The SVM is trained with a limited number of datapoints from the two train classes based on site spotting (Alexakis et al. 2021). The trained SVM then predicts the class labels of the remaining datapoints. This approach predicts the class of train with high accuracy – with only 12 incorrectly predicted labels out of 1116 test labels. The SVM approach offers an improved, data-driven approach to classifying trains without the need for “manual” labelling. Next, the SVM procedure is performed using three classes as the pattern presented in Fig. 6-left suggests three latent groups. The SVM predicted classes are illustrated in Fig. 6-right. The three groups are suspected to correspond to the three types of train class: (i) Class 185, (ii) Class 170, and (iii) Class 155/158, which is in accordance with site spotting.

The statistical relationship between $\hat{\beta}_2$ with the temperature and train class is modelled using a linear model. The linear model uses the temperature records and the class of train (one of the three classes predicted by the SVM) as inputs. The preliminary data are not used to fit this model. The expected $\hat{\beta}_2$ value from the fitted linear model is illustrated in Fig. 6-right. This model explains the data very well (e.g., R^2, a goodness-of-fit measure, of 95%).

The fitted linear model can be used to monitor deterioration at a sensor location using the following procedure:

1. Divide the full dataset into two separate sets: a training and test set;

2. Fit a linear model to the $\hat{\beta}_2$ values in the training dataset using the temperature and train class as input;

3. Compare the $\hat{\beta}_2$ predictions from the fitted linear model to the $\hat{\beta}_2$ values in the test dataset.

As an example, in Step 1 take the training set as the main set of data from the permanent FBG installation and the test set as the preliminary dataset. This selection was based on the preliminary observations by Alexakis et al. (2019a-c) that in five bridge locations, including 37NA6A7, the peak-to-peak amplitude of the dynamic strain response (e.g., Fig. 5) seemed to have been permanently increased between July 2016 (preliminary dataset) and the permanent sensing installation starting from November 2017 until today.

In Step 2, the train classes are given as one of three classes predicted by SVM. Here, we select the most frequent 3–carriage passenger train, Class 185.

In Step 3, the differences between the predicted and the test $\hat{\beta}_2$ values indicate changes in the dynamic deformation over time, by factoring out any seasonal effect, and in this case, the ambient temperature.

The results of this procedure implemented separately at the two symmetric quarter-span locations 37NA6A7 (backfill-backing crack) and 37NA3A4 (no visible deterioration) are presented in Fig. 7. At sensor 37NA6A7, Fig. 7-left, the clear separation between the predicted and the preliminary $\hat{\beta}_2$ values suggest a change in structural behaviour. This change corresponds to a peak-to-peak dynamic strain amplification of 32με. Note that the resolution of the y-axis is high enough to detect much smaller strain variations, e.g., below 5με, which corresponds to the dynamic strain variation due to only a typical daily temperature fluctuation of ~10ºC (Alexakis et al. 2019c). Conversely, at 37NA3A4 the deviation is small, indicating little evidence of any structural change, which is the case for all sensors, apart from the 5 locations indicated in Fig. 2 with dashed boxes. Note that some variation of the datapoints around the fitted curves is expected due to the stochastic nature of the data due to e.g. a varying number of passengers or unrecorded seasonal variations.

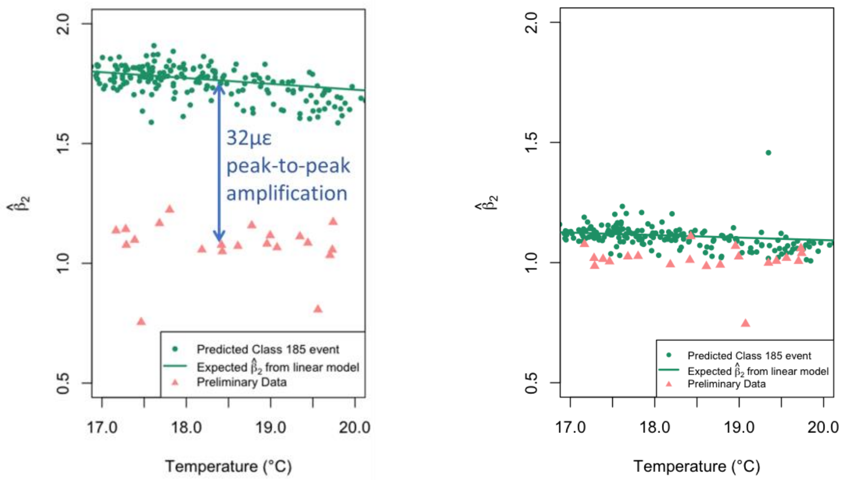

Figure 7. Comparison between the $\hat{\beta}_2$ estimates for the 2016 preliminary events and the predicted Class-185 curve (solid line given by the linear model) at sensor location 37NA6A7 (left) and 37NA3A4 (right).

The entire procedure involves: comparing events using a modified OPA approach, classifying train types using SVM, and monitoring deterioration by investigating changes in $\hat{\beta}_2$ values (strain amplification). This procedure provides a novel data-driven pipeline from sensor network data to structural health monitoring information.

4.3. The CFM-5 skewed arch bridge

4.3.1. Sensing network and installation novelties

The CFM-5 bridge is a single-span, skewed masonry arch railway bridge in North Yorkshire, UK. As shown in Fig. 8(a), it carries two lines of rail traffic over a highway. CFM-5 was built in 1868, primarily using stone masonry blockwork although its arch barrel is brickwork, laid helicoidally. The main damage is highlighted in Fig. 8(b) and consists of separation cracks between the arch and both spandrel walls, as well as a longitudinal crack on the east side of the arch approximately aligned with the centerline of the south rail track. This damage was addressed in a recent repair in 2016, in which the cracks were stitched at regular intervals and ten tie bars were installed through the bridge in its transverse direction. A key goal was to halt growth of the separation cracks and restore connectivity between the spandrels and arch, to reduce the magnitudes of dynamic arch movements in response to trains passing over the bridge. While this has succeeded, the duration over which the repairs will remain effective is unclear. This, in turn, has motivated SHM, although the project has also been used as an opportunity to evaluate a range of sensing technologies for broader application in masonry arch bridge monitoring (Cocking et. al 2019a).

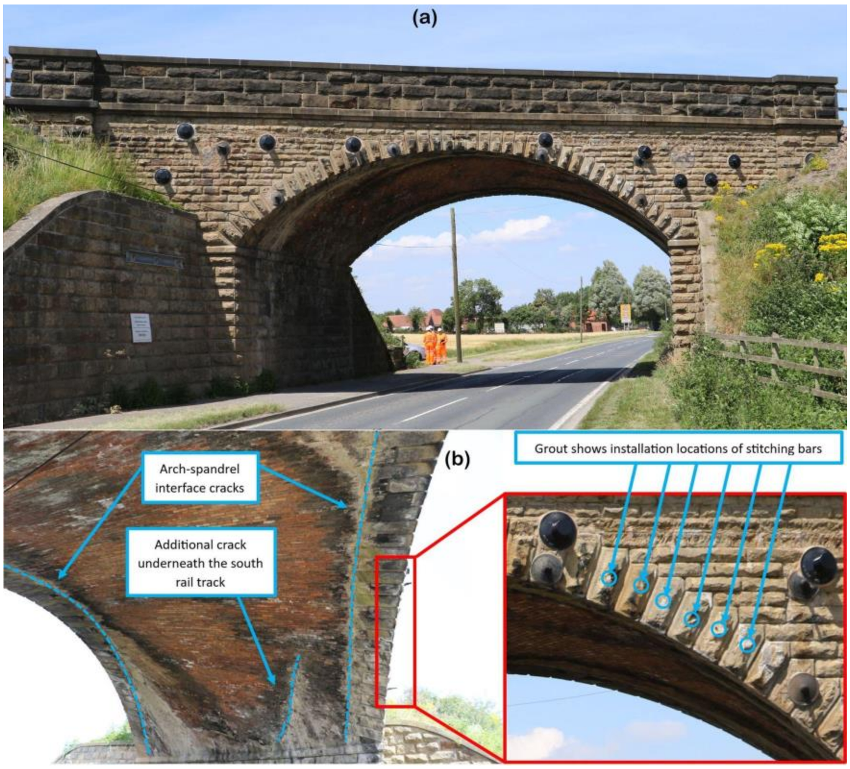

Figure 8. (a) Elevation view of the CFM-5 bridge, and (b) overview of the main cracking damage alongside indications of the recent repair work

Alongside other technologies (Cocking et. al 2019a), distributed arrays of FBGs were installed on the arch intrados of the CFM-5 bridge using aluminium clamps. Two novel methods were devised to implement these FBGs: (a) rosettes measuring dynamic principal strains, and hence the flow of force, through the arch barrel, and (b) 'FBG pairs' capturing multi-dimensional movements across the separation cracks. The full FBG installation is reported in Cocking (2021), which also describes complementary analyses leveraging videogrammetry and advanced laser scan analysis, alongside the FBG data.

As in Fig. 9, FBG rosettes measure a local strain state $\epsilon_{x,y}$ which can be converted, using the Mohr's circle of strain, to find the magnitudes and orientations of principal strains $\epsilon_{1,2}$ (details in Cocking et. al 2019b, and Cocking 2021). 'FBG pairs' consist of one FBG directly measuring in-plane crack opening, alongside a second which captures both in-plane and out-of-plane (shear) movements. Considering the geometry of the A-B-C triangle in Fig. 9(c), at each instance of time, dynamic shear deflections can be found (Cocking et. al 2021).

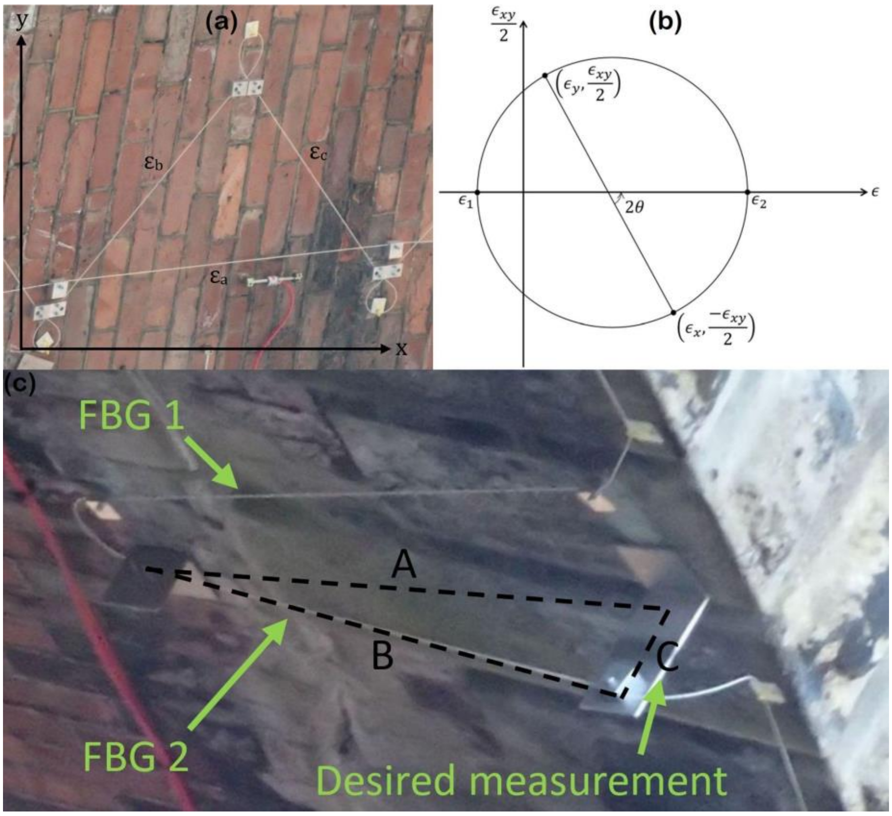

Figure 9. (a) An FBG strain rosette, from which dynamic principal strains are found using (b) the local Mohr's circle of strain, and (c) an 'FBG pair' measuring both in-plane (crack opening) and out-of-plane (shear) movements across a crack

4.3.2. Analysis and results

The 'FBG pairs' have revealed an asymmetric distribution of dynamic crack opening displacements that is consistent for common groups of train loading. The high sensitivity of FBGs enables precise characterization of distributed responses, such as these crack displacements and the in-plane arch strains, as well as the quantification of response sensitivity to external variables such as train speed, precise applied loading, and ambient temperature (Cocking et. al 2021, Cocking 2021, Cocking and DeJong 2022).

Fig. 10(a) shows the installation locations of the FBG rosettes R1 to R19, which are aligned with the northern rail track and longitudinal bridge centerline. Rosette R20 was damaged during installation and not ultimately used. Rotational symmetry in the arch response (demonstrated in Cocking 2021) allows for data from rosettes R1 to R19, measured for trains travelling on the south track, to be used to infer the response at 'imaginary' rosettes R20* to R30* when trains pass on the north track. In this way, distributions of the principal strains measured by FBG rosettes can be mapped across the extent of the arch barrel, to visualize the dynamic flow of force during train loading events.

Fig. 10(b) gives an example, in which the median distribution of instantaneous principal strains that are measured when the critical axles of TransPennine Express trains reach the FBG just to the east of the arch crown (marked with a green circle in Fig. 10(b)) are presented. A band of tensile (red) principal strains is observed to occur around this loading location, suggesting that the thrust line in this region of the arch is shifted towards the extrados. Compressive (blue) tensile strains are predominant outside of this region; this is consistent with the anticipated thrust line moving towards the intrados in these locations, particularly on the opposite side of the arch to the loading location. In general, the principal strains are approximately aligned with the skewed span direction, although in some places such as the north-eastern (top-right) quadrant of the bridge they are oriented towards the acute corner of the skewed arch.

Fig. 10(c) uses boxplots to show the statistical distribution of principal strains for the above loading instance. Data from 1,636 TransPennine Express trains have been included in this analysis, with 50% of these travelling on each of the northern and southern tracks. Plotted in dark blue, the dots in circles indicate median responses, thick bars represent the interquartile ranges (e.g., see ϵ_2 for rosette R17), and thin 'whiskers' show the data ranges excluding outliers. Outliers are plotted in cyan asterisks. The interquartile ranges are often too small to be visible, as the principal strain distributions are highly consistent for the majority of data. This indicates a stable response under repeated, common applied loading.

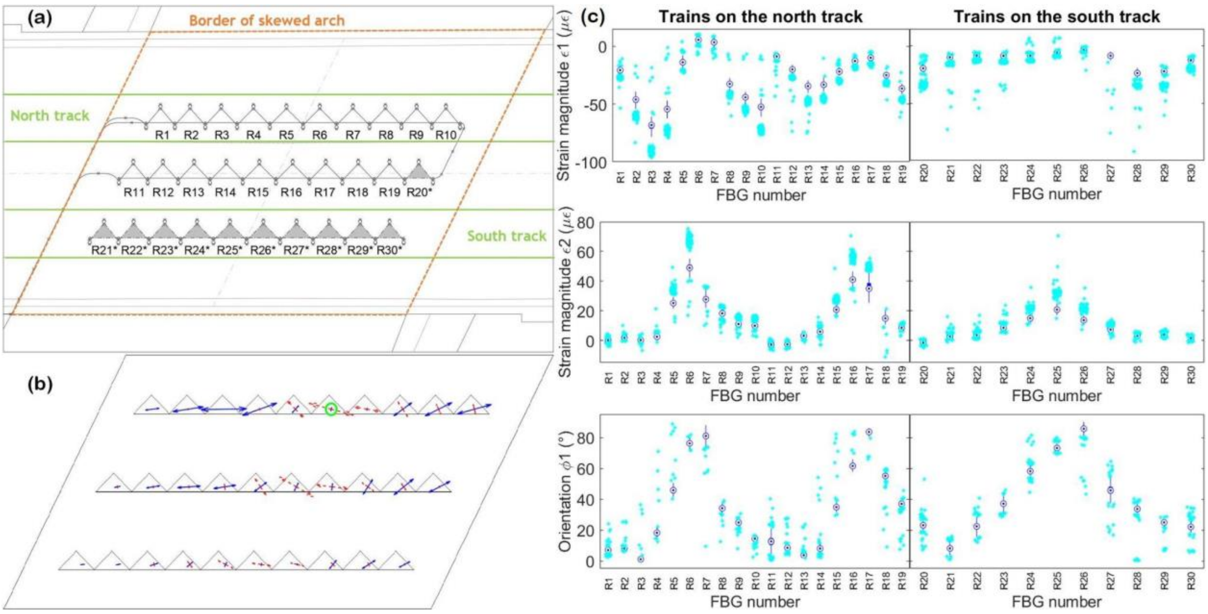

Figure 10. (a) FBG rosette installation plan for the CFM-5 bridge, (b) median principal strain distribution measured when the critical axles of TransPennine Express trains reach the arch

crown (green circle) with tensile and compressive principal strains shown in red and blue, respectively, and (c) boxplots showing the statistical distribution of principal strains ϵ_1 and ϵ_2 and orientation ϕ_1, for this loading instance.

It is hypothesized that damage, giving rise to local loss of stiffness, will manifest itself in the principal strain data as a permanent change in the force flow distribution. As already noted, FBGs are sensitive enough to detect damage at an early stage. Therefore, this FBG rosette system offers the means to track changes in the damage state of this bridge over time, as incipient or progressive damage occurs.

To the same end, Alexakis et al. (2020) conducted a parallel experimental study to the field monitoring of the two ageing railway bridges described in this and the previous sections, to describe the acoustic emission (AE) behavior of masonry under cyclic train loading. The study shows that AE sensors can capture increasing AE-energy data trends prior to local brittle failures, such as brick/mortar crushing, joint sliding and diagonal shear failures, which may not be reflected in the strain responses. This suggests that AE and FBG (dynamic strain) are complementary sensing techniques, with the potential, if combined, to provide a more comprehensive structural assessment at both the local and global response level. This idea has been the main motivation for the sensing deployment described in the following section.

4.4. Reinforced concrete half-joint motorway bridge

Half-joints are designed with a reduced section depth at the ends and were particularly favoured for car parks and bridges owing to a simplified design process and their suitability for precast construction. Despite the advantages, it has been found that this type of joint often deteriorates due to water seepage resulting in water stagnation in the nibs and ultimately corrosion of the reinforcement (Desnerck et al., 2016). In addition, in many cases they are particularly difficult to inspect as the inner part is not designed to be accessible. In the UK, the National Highways has implemented a dedicated management and inspection regime for half-joints to ensure risk mitigation and sufficient maintenance practices for deteriorated bridge decks with half-joints (English Highway Structures & Bridges Inspection & Assessment, 2020). Within this context, a reinforced concrete half-joint has been selected for monitoring purposes to evaluate the effectiveness of AE testing on damage detection and condition assessment during short and long-term field campaigns, which is complemented by environmental data and FBG-based dynamic strain sensing.

4.4.1. Sensing network and installation novelties

The selected half-joint is within the Strategic Road Network (SRN) in England and is located on a Class A motorway carrying traffic in four lanes, with a width of 15 m in each direction and a total width of approximately 40 m. Pictures of the bridge incorporating the half-joints are shown in Figure 11, taken during an inspection in December 2019. Access to the bearing shelf is limited on the monitored half-joint which is under an annual visual inspection regime by the asset operator. Its current condition is considered to be satisfactory[1].

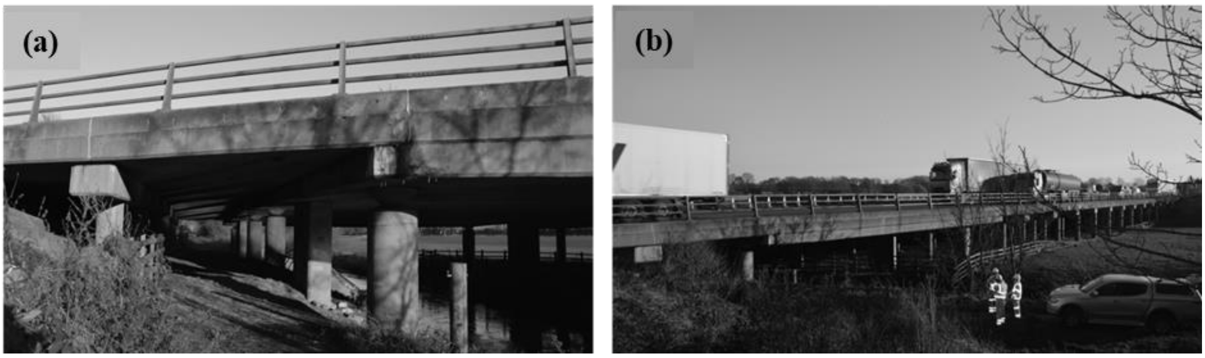

Figure 11: (a) Side Elevation of the bridge, (b) Traffic on the Northbound direction

The half-joint has been instrumented with a monitoring system comprising AE sensors, FBG strain and temperature sensors, and a weather station. The sensors were installed across the whole width of the half-joint covering both North and Southbound directions. A total of 24 piezoelectric AE sensors of the type PK6i were installed along the nib and the sides of the half-joint. The sensors have a resonant frequency of 55 kHz and an integral preamplifier of 26 dB. Behnia et al. (2014) suggests that this type of sensor has been shown to perform well on concrete bridges. The AE sensors form a linear array with a distance of 2 m between them, whereas the last two sensors were installed on the east side of the joint. A two-part rapid setting resin was used for acoustic coupling and a bolted clamp was used to ensure the sensors remain on the concrete surface. The array configuration was found to be appropriate to monitor the entire width of the bridge, taking into account the acoustic signal attenuation within the concrete body following calibration studies. Data are acquired continually with a sampling rate of 1 MHz using the commercially available Sensor Highway III (SH-III) system.

A Vaisala WXT530 series 6 weather station was installed and connected to SH-III to monitor weather parameters such as air temperature, rainfall accumulation and humidity. Four FBG-cable arrays of 20 sensors each, were installed along the half-joint. Three arrays were

[1] Personal communication with asset operator.

attached on the concrete surface using aluminium clamps to monitor strain in the longitudinal, transverse and vertical directions (corresponding to all three spatial directions) in a 2-m spacing along the half-joint. A fourth array was split in two with a 20 m extension and was attached on the east and west side of the joint. All the arrays were pre-tensioned to a minimum of 500 με. A sampling frequency of 50 Hz was found appropriate for monitoring. Each group of FBG sensors in 3-directions was installed adjacent to an AE sensor to ensure that AE data and strain can be correlated. A plan view of the location of AE and FBG sensors is shown in Figure 12a along with the locations of AE sensors on the East side (Figure 12b).

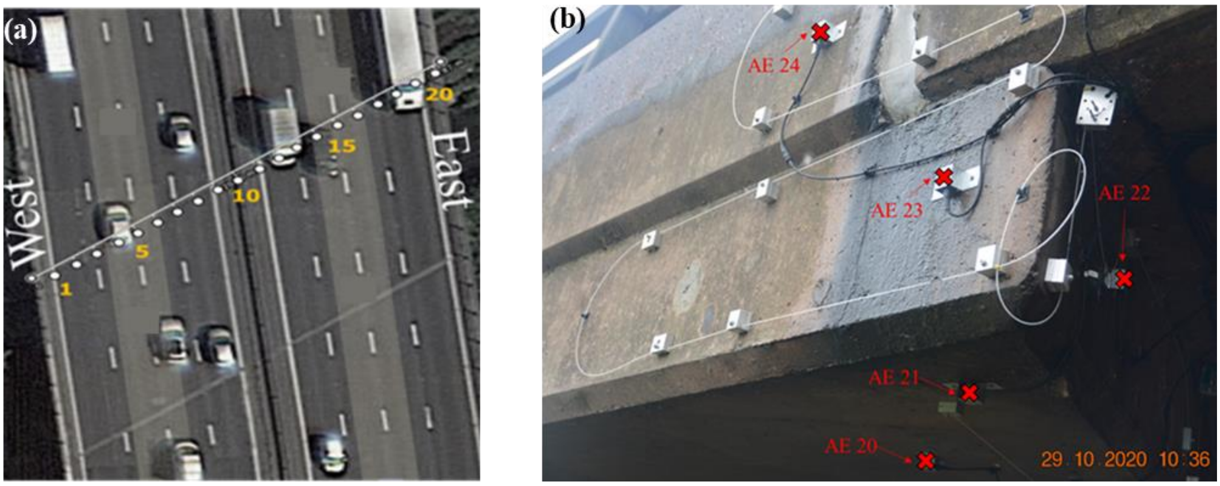

Figure 12: (a) Locations of AE and FBG sensors and (b) AE and FBG sensors on the half joint

Following successful installation of the AE sensors, a comprehensive calibration protocol was followed to ensure that the acoustic coupling between the sensors and the concrete surface is sufficient and also to determine the background noise, in order for an appropriate AE detection threshold to be set. The calibration was carried out during normal operating conditions using a HSU-Nielsen source as defined in EN 1330-9 (2017).

To verify the sensor sensitivity, pencil lead breaks were performed next to each individual sensor. Subsequently, pencil lead breaks were carried out at different locations and direction between sensors to obtain the attenuation of the elastic waves within the material. A series of calibrations tests was performed involving pencil breaks between consecutive AE sensors. Attenuation was investigated in the longitudinal and transverse directions for sensor AE 2 at fixed intervals of 50, 250, 500, 1000, 2000 mm (Figure 13a). The attenuation across the joint (vertical direction) was studied by performing centre punches at the drop in span. Lead breaks are shown in Figure 13b, where absolute energy is plotted against the recorded peak amplitudes. Such lead breaks are events of particularly high energy, imitating concrete cracking. Figure 13c shows the amplitude decay in the longitudinal directions against distance from sensor AE 2. The indicative pencil breaks between sensors AE 1, 2, 19, 20 are also shown (Figures 13d, e)

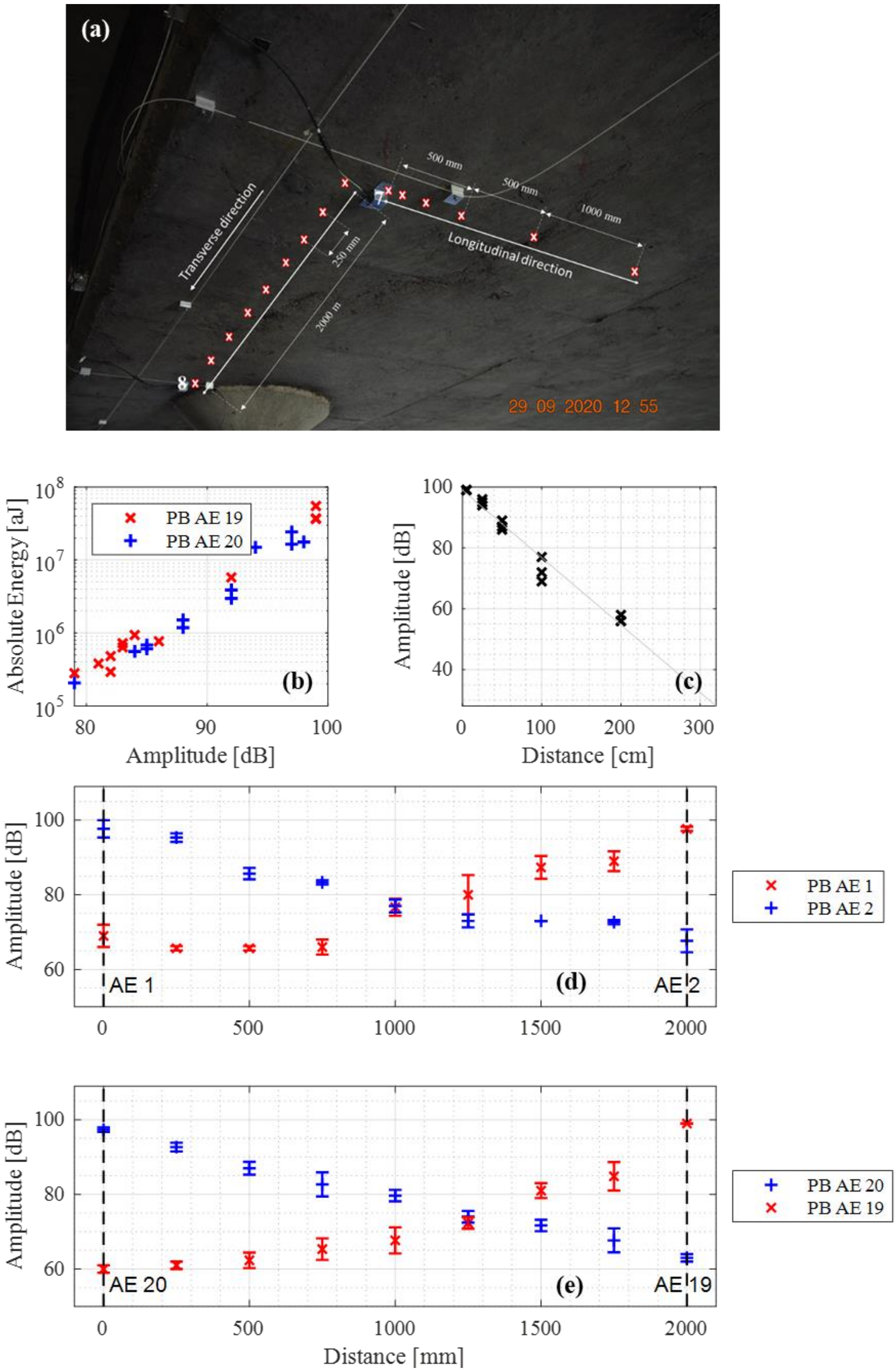

Figure 13: Calibration of Acoustic Emission sensors. (a) Locations of transverse and longitudinal pencil breaks, (b) Indicative correlation between Absolute Energy and Amplitude, (c) Longitudinal attenuation from sensor AE 2, (d-e) Indicative pencil breaks between sensors AE 1, 2, 19, 20

4.4.2. Analysis and results

The overall strain distribution from the vertical FBG sensors is shown in Figure 14. Each line in the boxplot, corresponds to the median value of the peak strain recorded per 5 minute interval for September 2020 at each sensor location, whereas the box limits define the 25th and 75th percentiles. The corresponding sensor locations are given in Figure 11a. It is shown that the strains are distributed symmetrically. Lane one, highlighted in light blue, carries the heaviest traffic, with similar average peak strains recorded for both traffic directions.

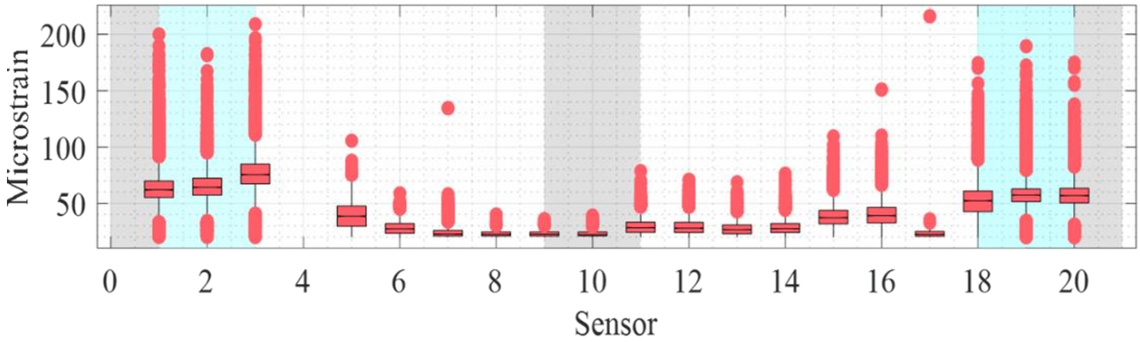

Figure 14: Boxplots of strain data for each FBG sensor from array 3 during September 2020. Blue regions indicate the lanes with the heavier traffic

For in-service bridges, recorded AE hits are emitted due to traffic, noise and/or deterioration processes, given that the bridge is continually under load, which is the fundamental principle for acoustic waves being emitted. Hence, one needs to distinguish between different sources, although preliminary findings can be extracted by looking at the total number of AE hits recorded from each sensor. Taking into account the calibration tests, the AE data were pre-processed by removing AE hits with a peak amplitude below 59 dB. Furthermore, only hits with counts larger than 5 and less than 10,000 were considered. This further increase of the threshold was justified from the attenuation data, where the minimum amplitude recorded at the maximum distance between two sensors was 60 dB. In addition, all hits with zero energy were also removed as this commonly represents spurious data rather than useful data (Tziavos et al., 2020). It was found that the majority of hits with zero energy were below 60 dB.

The AE activity on the half-joint expressed by the total number of recorded hits is given in Figure 15. The presented data, collected during September 2020 (Figure 15a), confirm that AE activity is dependent on the stresses applied on the bridge, as expected. It is also apparent that the AE sensors installed underneath the first lanes in each direction recorded a higher number of hits, indicating that larger stressors on the half-joint were responsible for the higher activity. Although AE hits are consistently higher in the same locations for both northbound and southbound directions, for the latter it is shown that a significantly higher number of hits were recorded, particularly for AE 19.

In Figure 15b the number of hits recorded by each sensor for the first four months of acquisition is illustrated. A total of 17 days of continuous monitoring for each month are included. The findings from September are further confirmed for the subsequent months, indicating that the AE activity is significantly higher on the first two lanes of the southbound direction. This is despite the fact that the recorded peak strains from the FBG sensors are consistent between the two lanes. A further deduction from these two figures is that AE can be also used for short-term monitoring campaigns in order to provide structural engineers with a preliminary analysis on the activity on the structure under in-service conditions, as areas of higher AE activity are commonly associated with deterioration mechanisms as the environmental and traffic influence on both lanes is found to be similar.

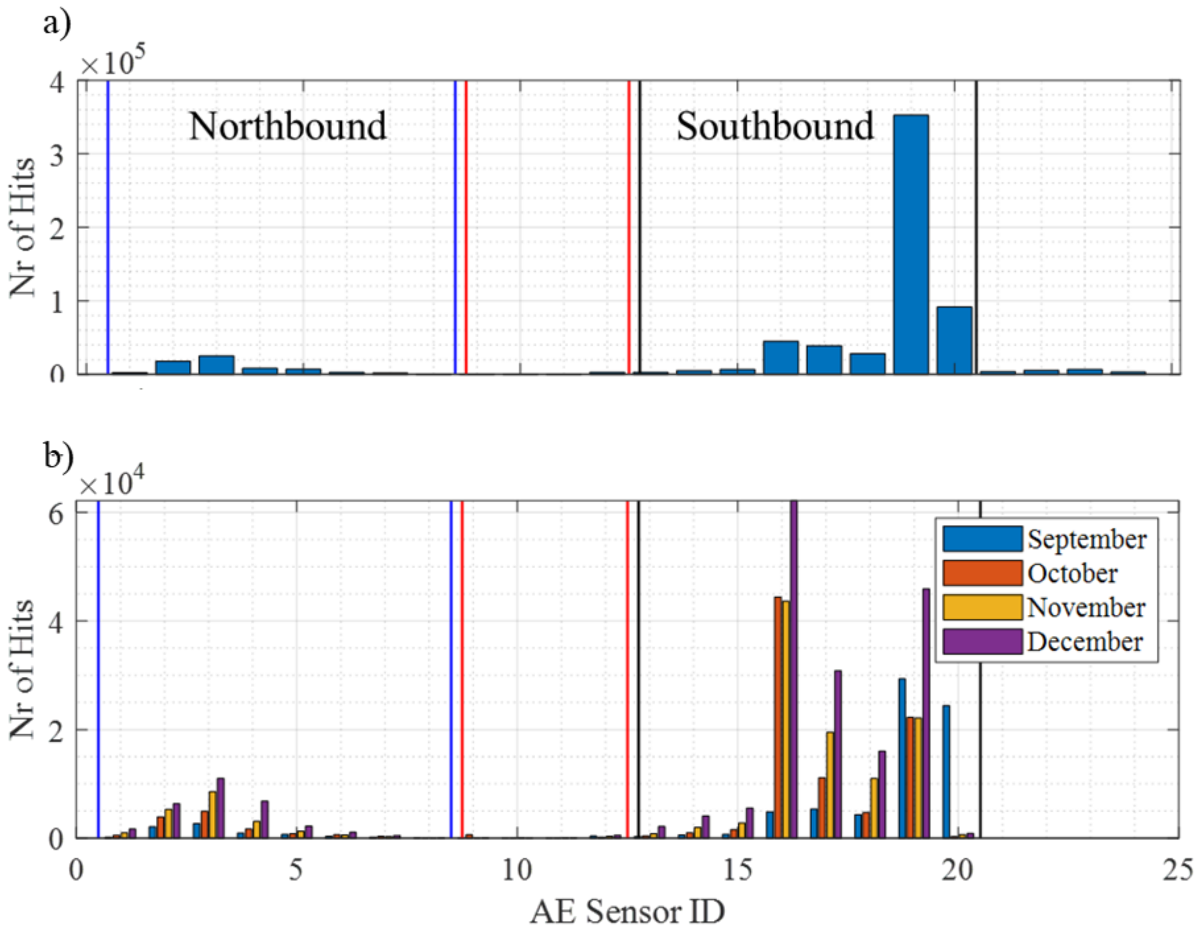

Figure 15: Number of hits per channel along the AE array for Northbound and Southbound directions for a) September and b) September – December

4.5. Conclusions

This chapter summarises results from three ageing bridge monitoring projects. In all cases, the sensing networks installed cover large areas with high densities of sensing points, monitoring multiple aspects of the structural response at both the local and global level.

FBG networks are installed in different configurations with the use of aluminium clamps. This technique has been proven to be robust during long monitoring periods (5 years so far) and allows versatility in installation. In particular, the technique allows: (i) flexibility in choosing the in-plane sensing direction (e.g. to adjust to a particular cracking pattern or imminent failure mechanism), (ii) the formation of consecutive strain rosettes (e.g. to study the force flow within arch barrels), (iii) out-of-plane displacement monitoring (e.g. to study arch ‘pumping’), and (iv) altering the sensing physical parameter per FBG location (i.e. to choose between dynamic strain and ambient temperature).

Furthermore, FBG data from selective locations can be used for loading classification (e.g. identification of train speed, class and direction). When statistical shape analysis was enhanced with a support vector machine, small changes in response due to slight loading and temperature variations could be distinguished, showing potential to detect mechanical deterioration that alters locally the dynamic strain response below any thermal effect.

Analysis of the AE field data of the concrete bridge has identified locations of higher AE activity compared to other symmetric locations of similar loading and dynamic strain response, as shown by the FBG data. This indicates even when FBG data may not detect a difference in strain, complementary AE sensing may help in detecting underlying deterioration, though this requires further research for validation. Experimental studies on the AE behaviour of masonry under cyclic loading that were conducted in parallel with the field installations, confirm the detection of data trends that are not necessarily shown in strain data, especially for brittle failure modes. On the other hand, while AE sensing alone may enhance the information locally, without FBG sensing it is difficult to interpret. FBG and AE sensing seem to be highly complementary techniques, and creating unified systems that integrate statistical modelling may enhance further the damage assessment of complex deteriorating systems.

CHAPTER 4

Acknowledgements

The Marsh Lane bridge monitoring project has been funded by the Lloyd's Register Foundation, EPSRC and Innovate UK through the Data-Centric Engineering programme of the Alan Turing Institute and through the Cambridge Centre for Smart Infrastructure and Construction (CSIC). Additional funding for IT equipment was provided to the first author by the School of Engineering & Applied Science and the Aston Institute of Urban Technology and the Environment (ASTUTE), Aston University (budget codes 10068 and 10630). The CFM-5 bridge monitoring project has been funded by Network Rail (NR) and EPSRC via the Doctoral Training Partnership (Grant Number EP/M506485/1). The half-joint bridge monitoring project has been funded by Highways England (HE).

The monitoring installation in all three bridges was performed with assistance from the CSIC, supported by EPSRC, Innovate UK, and industry funding (including Grant Numbers EP/I019308/1, EP/K000314/1, EP/L010917/1, and EP/N021614/1).

The authors are grateful to NR, HE, AECOM and KIER for supporting the sensing deployment and would like to acknowledge the special contribution of Ian Billington (HE), Robert Dean, Christopher Heap, Sam De'Ath (NR), David Kite (AECOM), Cedric Kechavarzi (CSIC) and their supporting teams, without which this study wouldn't have been possible.

References

Acikgoz, S., Soga, K. and Woodhams, J. 2017. Evaluation of the response of a vaulted masonry structure to differential settlements. *Constr Build Mater*, 150, 916–931.

Acikgoz, S., DeJong, M. J., and Soga, K. 2018a. Sensing dynamic displacements in masonry rail bridges using 2D digital image correlation. *Struct Control Hlth*, 25,e2187.

Acikgoz, S., DeJong, M. J., Kechavarzi, C. and Soga, K. 2018b. Dynamic response of a damaged masonry rail viaduct: Measurement and interpretation. *Eng Struct*, 168, 544–558.

Alexakis, H., Franza, A., Acikgoz, S., and DeJong, M. J. 2019a. Structural Health Monitoring of a masonry viaduct with Fibre Bragg Grating sensors, *IABSE SYMPOSIUM GUIMARÃES 2019, Towards a Resilient Built Environment Risk and Asset Management*, pp. 1560-1567.

Alexakis, H., Franza, A., Acikgoz, S. and DeJong, M. J. 2019b. A multi-sensing monitoring system to study deterioration of a railway bridge, *9th International Conference on Structural Health Monitoring of Intelligent Infrastructure (SHMII-9), St. Louis, Missouri, USA*.

Alexakis, H., Franza, A., Acikgoz, S. and DeJong, M. J. 2019c. Monitoring bridge degradation using dynamic strain, acoustic emission and environmental data, *International Conference on Smart Infrastructure and Construction*, *University of Cambridge.*

Alexakis, H., Liu, H. and DeJong, M. J. 2020. Damage identification of brick masonry under cyclic loading based on acoustic emissions. *Eng Struct* 221**,** 110945.

Alexakis, H., Lau, F.D.H. and DeJong, M. J. 2021. Fibre optic sensing of ageing railway infrastructure enhanced with statistical shape analysis. *J Civil Struct Health Monit* 11, 49–67

Behnia, A., Chai, H. K., and Shiotani, T. 2014. Advanced structural health monitoring of concrete structures with the aid of acoustic emission. *Constr Build Mat*, 65, 282–302.

British Standards Institution – BSI, 1962. *Amendment No. 4 (PD 4639) to BS 153-3B4:1958 Specification for steel girder bridges, London: BSI*

Calvi, G.M., Moratti, M., O'Reilly, G.J., Scattarreggia, N., Monteiro, R., Malomo, D., Calvi, P.M. and Pinho, R. 2019. Once upon a time in Italy: The tale of the Morandi Bridge. *Structural Engineering International*, 29, 198–217.

Chaiyasarn, K. et al. 2018. Crack detection in masonry structures using convolutional neural networks and support vector machines. *35th ISARC, Berlin, Germany*, 118–125.

Cocking, S., Thompson, D., and DeJong, M. J. 2019a. Comparative Evaluation of Monitoring Technologies for a Historic Skewed Masonry Arch Railway Bridge, *ARCH 2019, the 9th International Conference on Arch Bridges, Porto, Portugal*, 439–446.

Cocking, S.H., Ye, C., and DeJong, M. J. 2019b. Damage Assessment of a Railway Bridge using Fibre Optic Sensing and LiDAR Data, *ICSIC 2019, the International Conference on Smart Infrastructure and Construction, Cambridge, UK*.

Cocking, S. 2021. Dynamic distributed monitoring of masonry railway bridges (PhD thesis), University of Cambridge, UK.

Cocking, S., Alexakis, H., and DeJong, M. J. 2021. Distributed dynamic fibre-optic strain monitoring of the behaviour of a skewed masonry arch railway bridge. *J Civil Struct Health Monit* 11, 989–1012.

Cocking, S. and DeJong, M. J. 2022. Long-Term Structural Monitoring of a Skewed Masonry Arch Railway Bridge Using Fibre Bragg Gratings, *EWSHM 2022, the 10th European Workshop on Structural Health Monitoring*.

Cortes, C. and Vapnik, V. 1995. Support-vector networks. Machine learning, 20, 273–297.

De Santis, S. and Tomor, A. K. 2013. Laboratory and field studies on the use of acoustic emission for masonry bridges. *NDT&E Int*, 55, 64–74.

Desnerck, P., Lees, J. M. and Morley, C. T. 2016. Impact of the reinforcement layout on the load capacity of reinforced concrete half-joints. *Eng Struct*, 127, 227–239.

Dryden, I. and Mardia, K. 2016. *Statistical Shape Analysis: With Applications in R. Wiley Series in Probability and Statistics, Wiley.*

EN 1330-9. 2017. Non-destructive testing - *Terminology - Part 9: Terms used in acoustic emission testing, Comité Européen de Normalisation*, 1-13.

English Highway Structures & Bridges Inspection & Assessment. 2020. *CS 466. Risk management and structural assessment of concrete half-joint deck structures* (formerly IAN 53/04 and BA 39/93 (plus part of BD 44/15)).

Kaloop, M. R. and Hu, J. W. 2015. Stayed-cable bridge damage detection and localization based on accelerometer health monitoring measurements. *Shock Vib*, 102682.

Mutsuyoshi, H. 2001. *Present situation of durability of post-tensioned PC bridges in Japan*, Bulletin-Fib.

Orbán, Z. 2004. Assessment, reliability and maintenance of masonry arch railway bridges in Rurope. *ARCH'04, Barcelona*.

Santos, J. P., Cremona, C., Calado, L., Silveira, P., and Orcesi, A. D. 2016. On-line unsupervised detection of early damage. *Struct. Control Health Monit*. 23, 1047–1069.

Tziavos, N. I., Hemida, H., Dirar, S., Papaelias, M., Metje, N. and Baniotopoulos, C. 2020. Structural health monitoring of grouted connections for offshore wind turbines by means of acoustic emission: An experimental study. *Renewable energy*, 147, 130-140.

UIC 778-4. 2009. *Defects in railway bridges and procedures for maintenance*. UIC Code 778-4 R, 2nd Ed., International Union of Railways, Paris, 32.

United Nations. 2017. *Resolution adopted by the General Assembly on 6 July 2017*, A/RES/71/313